1-1-2019

# P2-type Na2/3Ni1/3Mn2/3O2as a cathode materialwith high-rate and long-life for sodium ionstorage

Qiannan Liu
*Wenzhou University, University of Wollongong*, qiannan@uow.edu.au

Zhe Hu
*University of Wollongong*, zh865@uowmail.edu.au

Mingzhe Chen
*University of Wollongong*, mc800@uowmail.edu.au

Chao Zou
*Wenzhou University*

Huile Jin
*Wenzhou University*

*See next page for additional authors*

# P2-type Na2/3Ni1/3Mn2/3O2as a cathode materialwith high-rate and long-life for sodium ionstorage


## Abstract

Layered P2-type Na 2/3 Ni 1/3 Mn 2/3 O 2 was successfully synthesized through a facile sol-gel method and subsequent heat treatment. Resulting from different phase transformation and sodium ion diffusion rates, its electrochemical performance is highly related to the cut-off voltage and the electrolyte used. When the cut-off voltage is set up to 4.5 V or lowered to 1.5 V, capacity fade happens due to the occurrence of P2-O2 transformation and electrolyte decomposition or the redox reaction of the Mn 4+ /Mn 3+ ionic pair and P2-P2' transformation. The electrode maintained 89.0 mA h g -1 with good cycling stability and excellent structural preservation between 4.0 and 2.0 V. The capacity retention is 71.2% even after 1200 cycles at 10C. It can be expected that P2-type Na 2/3 Ni 1/3 Mn 2/3 O 2 is very promising as a cathode material for sodium ion batteries.



## Keywords

sodium, long-life, high-rate, materialwith, cathode, na2/3ni1/3mn2/3o2as, ionstorage, p2-type


## Disciplines

Engineering | Physical Sciences and Mathematics


## Publication Details

Liu, Q., Hu, Z., Chen, M., Zou, C., Jin, H., Wang, S., Gu, Q. & Chou, S. (2019). P2-type Na2/3Ni1/3Mn2/3O2as a cathode materialwith high-rate and long-life for sodium ionstorage. Journal of Materials Chemistry A, 7 (15), 9215-9221.



## Authors

Qiannan Liu, Zhe Hu, Mingzhe Chen, Chao Zou, Huile Jin, Shun Wang, Qinfen Gu, and Shulei Chou

# P2-type $Na_{2/3}Ni_{1/3}Mn_{2/3}O_2$ as cathode materials with high-rate and long-life for sodium ion storage

Qiannan Liu,[1,2] Zhe Hu,[2] Mingzhe Chen,[2] Chao Zou,[*,1] Huile Jin,[1] Shun Wang,[1] Qinfen Gu,[3] and Shulei Chou[*,2]

[1] *College of Chemistry and Materials Engineering, Wenzhou University, Wenzhou, Zhejiang 325027, China. Email: zouchao@wzu.edu.cn*
[2] *Institute for Superconducting and Electronic Materials, Australian Institute for Innovative Materials, Innovation Campus, University of Wollongong, Squires Way, North Wollongong, NSW 2522, Australia. Email: shulei@uow.edu.au*
[3] *Australian Synchrotron, 800 Blackburn Road, Clayton, VIC 3168, Australia*
*Electronic Supplementary Information (ESI) available: [details of any supplementary information available should be included here]. See DOI: 10.1039/x0xx00000x*

Layered P2-type $Na_{2/3}Ni_{1/3}Mn_{2/3}O_2$ was successfully synthesized through a facile sol-gel method and subsequent heat treatment. Resulting from different phase transformation and sodium ion diffusion rate, its electrochemical performance is highly related to the cut-off voltage and the electrolyte used. When the cut-off voltage is set up to 4.5 V or lowered to 1.5 V, capacity fade happens due to the occurrence of P2-O2 transformation and electrolyte decomposition or the redox reaction of the $Mn^{4+}/Mn^{3+}$ ionic pair and P2-P2' transformation. The electrode maintained 89.0 mAh $g^{-1}$ with good cycling stability and excellent structural preservation between 4.0-2.0 V. The capacity retention is 71.2% even after 1200 cycles at 10 C. It can be expected that P2-type $Na_{2/3}Ni_{1/3}Mn_{2/3}O_2$ is very promising as a cathode material for sodium ion battery.

## Introduction

The demand for large-scale energy storage systems has been growing significantly due to the requirement for the applications such as smart grid. Among the diverse energy storage technologies, the secondary rechargeable battery is one of the most promising techniques to store electricity on a large-scale.[1-3] Due to the low cost and abundant sources of sodium, the sodium ion batteries (SIBs) may have the potential to replace lithium ion batteries and meet the increasing demand for electric devices, and has attracted more and more attentions.[4-8] Nevertheless, the large diameter of the $Na^+$ ion makes it difficult to find suitable host materials for rapid $Na^+$ extraction and insertion due to the sluggish reaction kinetics. It is highly essential to develop effective cathodes for high performance SIBs with sufficient Na storage ability, high rate capability, and long-term cycling stability.

Researches on cathode materials for SIBs have been focused on compounds ranging from polyanions to layered transition metal oxides,[9-11] and it is suggested that layered sodium transition metal oxides show outstanding electrode properties. Moreover, the barrier for $Na^+$ migration can potentially be lower than that for $Li^+$ migration in the layered structures and the higher vacancy concentrations of sodium layered oxides can offer larger capacity.[12-13] Layered sodium transition metal oxides are classified into several groups such as O3- and P2-types based on the location of the Na-ions (O: octahedral and P: prismatic).[7, 14] It is reported that P2-structured sodium intercalated materials show better Na storage and cyclability than O3-featured ones owing to the larger residing sites for sodium ions, less favourability in phase transition and faster ion diffusion in trigonal prismatic environment vs. octahedral one.[15-18] Layered sodium manganese bronzes, $Na_xMn_{1-y}M_yO_2$ (A = Co, Ni, Fe, *etc.*) with the P2-structure, normally with high Na storage capacity, have been studied by many researchers. Among those, $Na_xMn_{1-y}Ni_yO_2$ and some metal substituted or doping materials, have been widely studied since last century due to the high operating voltage based on a $Ni^{2+}/Ni^{4+}$ redox reaction,[19-28] including the $Na_{2/3}Ni_{1/3}Mn_{2/3}O_2$,[23] $NaNi_{0.5}Mn_{0.3}Ti_{0.2}O_2$,[24] $Na_{0.5}Ni_{0.25}Mn_{0.75}O_2$,[25] $Na_{0.67}Mn_{0.60}Ni_{0.30}Co_{0.10}O_2$,[26] $Na_{0.67}Ni_{0.3-x}Cu_xMn_{0.7}O_2$,[27] and $Na_{0.67}Ni_{0.23}Mg_{0.1}Mn_{0.67}O_2$[28] *et al*. For the primary $Na_{2/3}Ni_{1/3}Mn_{2/3}O_2$ (NNMO), all 2/3 of Na ions can be reversibly extracted and intercalated to the host structure providing specific capacity of 173 mAh $g^{-1}$ (1 C = 173 mA $g^{-1}$).[29] Moreover, water cannot be intercalated into the $Na_{2/3}Ni_{1/3}Mn_{2/3}O_2$ framework due to the existence of superlattice ordering Ni atoms within the transition metal layer which apparently induces a very strong interlayer interaction and inhibits the uptake of water.[30] When applied for solid-state SIBs, the NNMO showed a superior stability and high reversibility with a capacity retention of 90% after 10 000 cycles at 6 C.[31] However, good cycling stability can only be obtained with cut-off voltage below 4.0 V due to the phase transformation from P2-O2 above 4.1 V.

In this paper, layered P2-type $Na_{2/3}Ni_{1/3}Mn_{2/3}O_2$ was successfully synthesized and further studied as a cathode material for SIB. The effect of cut-off voltages, current density and FEC additive on the cycling stability and coulombic efficiency were discussed in detail. *In situ* XRD and galvanostatic intermittent titration technique (GITT) were also used to better understand the mechanism and sodium ion diffusion during the sodium intercalation and deintercalation process, which provide solid experimental evidence of the structural evolution upon cycling tests under different cut-off voltages. Resulting from different phase transformation and sodium ion diffusion rate, the electrochemical performance is highly related to the cut-off voltage and the electrolyte used. The prepared P2-$Na_{2/3}Ni_{1/3}Mn_{2/3}O_2$ exhibited an initial discharge capacity as high as 179.7 mAh $g^{-1}$ when cycling between 4.5-2.0 V. However, great capacity fading was observed in this voltage area. In the voltage range of 4.0-1.5 V, the electrode exhibited an

initial capacity of 151.0 mAh $g^{-1}$ with slight capacity fading due to the structure distortion caused by the Jahn-Teller $Mn^{3+}$ ions. When cycling in the range of 4.0-2.0 V, the electrode maintained 89.0 mAh $g^{-1}$ with good cycling stability and excellent structural preservation. The capacity retention is 71.2% even after 1200 cycles at 10 C.

## Experimental

***Material Preparation.*** $Na_{2/3}Ni_{1/3}Mn_{2/3}O_2$ (NNMO) powders were synthesized through a facile sol-gel method. All the chemicals were used as purchased. Sodium nitrate, nickel nitrate hexahydrate and manganese nitrate tetrahydrate with mole ratio of 2.08/1/2 were dissolved successively in deionized water to form a uniform solution. After stirring for 30 minutes, the mixed solution was added dropwise into 20 ml of ethylene glycol under continuous stirring. Then, the obtained mixture was heated at 80°C to form a gel precursor, which was then heated in a muffle furnace at 800, 850, or 900°C for 20 h in air to obtain the final products after naturally cooling to room temperature.

***Structural Characterization.*** The morphologies of the as-prepared samples were investigated by field-emission scanning electron microscopy (FESEM, JEOL JSM-7500) and transmission electron microscopy (TEM, JEOL ARM 200F). TEM samples were prepared after sonication treatment. The microstructures of the as-prepared powders were characterized on a synchrotron X-ray diffraction beamline with a wavelength (λ) of 0.6885 Å calibrated with the National Institute of Standards and Technology (NIST) $LaB_6$ 660b standard reference material and laboratory X-ray diffraction (XRD, GBC MMA diffractometer) with Cu $K_\alpha$ radiation. Mn and Ni K-edge X-ray absorption near the edge structure (XANES) was performed at Pohang Accelerating Laboratory in Republic of Korea using a double Si (111) monochromator. All spectra were normalized to the main edge jump.

***Electrochemical Measurements.*** The electrodes were prepared by mixing 80 wt% active materials, 10 wt% Super P, and 10 wt% polyvinylidene fluoride (PVDF) binder to form a slurry, which was then coated on an aluminium foil. Next, the aluminium foil was dried in a vacuum oven overnight at 120°C. After that, the working electrodes were cut out and pressed under a pressure of 20 MPa. The electrolyte used was 1.0 mol $L^{-1}$ $NaClO_4$ in an ethylene carbonate (EC) – diethyl carbonate (DEC) solution (1:1, v/v) with or without 3% fluoroethylene carbonate (FEC) additive. Sodium foil was cut from a sodium bulk stored in mineral oil and used as both the counter and reference electrodes. The cells were assembled in an argon-filled glove box. The electrochemical performances were tested on a Land Test System at different current densities. Cyclic voltammetry (CV) at a scan rate of 0.1 mV s-1 and electrochemical impedance spectroscopy (EIS) from 100 kHz to 100 mHz were performed using a CHI 660b electrochemistry workstation. The diffusion coefficient of Na+ ions was studied using the galvanostatic intermittent titration technique (GITT). For the GITT measurement, the cells were charged and discharged at 0.1 C for 360 s followed by an open circuit relaxation for 1 h. All the electrochemical tests were conducted at room temperature.

## Results and discussion

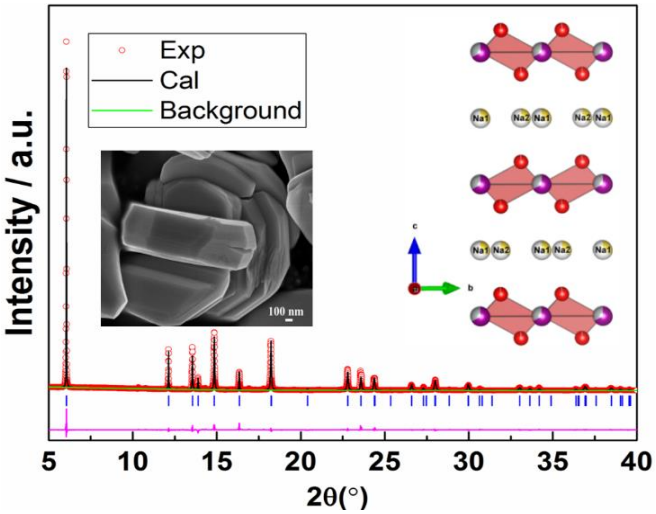


**Figure 1.** XRD pattern and SEM image (inset) of the as-prepared NNMO (wavelength=0.05899 nm).

The XRD Rietveld refinement of the P2-$Na_{2/3}Ni_{1/3}Mn_{2/3}O_2$ prepared at 850℃ was performed, and the refinement results and SEM image are listed in **Figure 1**. The powders obtained are pure NNMO, whose peaks can be indexed to the hexagonal phase system with space group P63/mmc.[32] The *a* and *c* parameters are refined to be 2.885 and 11.155 Å, respectively. All the peaks are sharp

and well defined, indicating high crystallinity of the prepared sample. The values of the refined structure parameters are shown in Table S1 in the supporting information. From the SEM image shown inset, it can be seen that uniform plate-shaped NNMO, in thickness of ~500 nm and diameter of ~1 μm, were formed. The calcination temperature plays an important role in the synthesis of pure and image-defined NNMO. XRD patterns and morphologies of NNMO powders prepared at different temperatures are shown in Figure S1 and Figure S2 in the supporting information, respectively. All the samples show good crystallinity. When calcined at lower temperature of 800℃, the obtained powders are NNMO with plenty of $Na_{0.91}NiO_2$ impurities. Further increasing the calcination temperature to 900℃, $Na_{0.7}MnO_2$ impurities are formed instead. Powders obtained at 800℃ were irregular and did not have a defined image. Although the surface looked to be smooth, the plates consisted of different layers, which can be seen in the high magnification images. The powders grow to be bigger and thicker after calcination at 900°C. The TEM image and SAED pattern of NNMO prepared at 850°C in Figure S3 further demonstrates its layered structure and good crystallinity.

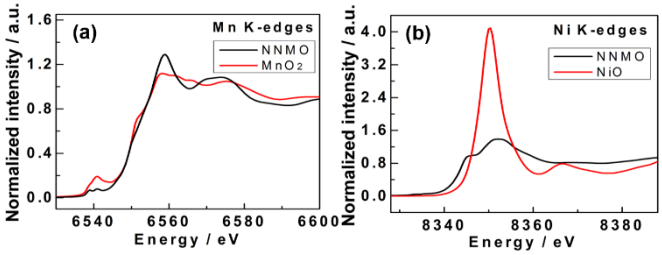


**Figure 2**. X-ray absorption near the edge structure (XANES) of as-prepared NMMO powders: (a) Mn K-edges and (b) Ni K-edges.

To determine the valence state of Mn and Ni in NNMO, XANES was conducted and is shown in **Figure 2**. The XANES of $MnO_2$ and NiO are also shown as references. It can be seen that the spectrum of Mn in NNMO corresponds well with that of $MnO_2$. Slow cooling leads to the oxygen uptake during the cooling process and presence of manganese vacancies thus a higher concentration of $Mn^{4+}$ which suppresses the cooperative Jahn–Teller distortion.[33-34] The pre-edge peaks in the spectra are indicative of structural distortion in the $MnO_6$ octahedra.[35] Moreover, Ni in NNMO can be determined to stay at +2 valence based on the spectrum of NiO. Thus the Ni and Mn are at +2 and +4 state respectively in NNMO, which is in agreement with previous reports.[36-37] And it can be predicted that in the bifunctional transition-metal layer, $Ni^{2+}$ acts as a double redox-active centre and $Mn^{4+}$ provides stability to the host structure.[38]

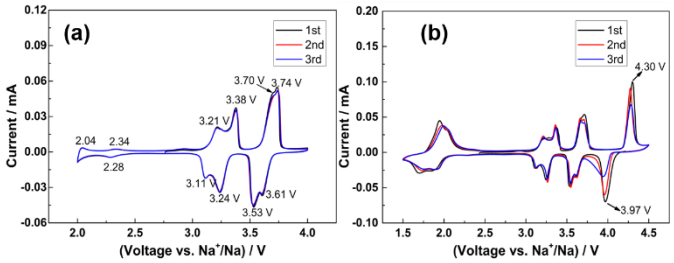


**Figure 3**. Cyclic voltammetry curves of Na/NNMO cells at different cut-off voltages: (a) 4.0-2.0 V and (b) 4.5-1.5 V.

The cyclic voltammetry curves of Na/NNMO cells (corresponding to sodium deintercalation/intercalation from/into $Na_{2/3}Ni_{1/3}Mn_{2/3}O_2$, respectively) of Na/NNMO cells with different charge–discharge cut-off voltages are shown and compared in **Figure 3**. The charge–discharge cut-off voltages are set to 4.0/2.0 and 4.5/1.5 V, respectively, to study the phase change happening until high voltage of 4.5 V or low voltage of 1.5 V. A series of complicated CV peaks have been observed, indicating a multitude of possible phase transitions accompanying with the de-insertion or insertion of $Na^+$ ions.

When cycling between 4.0 and 2.0 V, six highly reproducible pairs of peaks, having positions centred at 2.04/2.00, 2.34/2.28, 3.21/3.11, 3.38/3.24, 3.70/3.53, 3.74/3.61 V vs. $Na^+$/Na respectively of Na/NNMO cell were observed in the CV curves (Figure 3a). The four redox peaks between 3.0-4.0 V are associated with the transition of $Ni^{2+}$-$Ni^{3+}$-$Ni^{3.5+}$ along with $Na^+$ extraction/insertion processes.[39] The various minor plateaus between 2.0-3.0 V during the processes come from $Na^+$/vacancy ordering sequence or transitions involving the gliding of oxygen planes.[40-41] Mn ions stay at +4 state and are electrochemically inert above 2.0 V, which can help effectively maintain the structural stability in the absence of Jahn-Teller active $Mn^{3+}$, therefore leading to the stabilisation of the undistorted P2 hexagonal crystal structure. The overlapped anodic and cathodic peaks demonstrated the electrochemical stability of NNMO between 4.0- 2.0 V.

Further sweeping to 4.5 V, a new pair redox peak of 4.30/3.97 V was observed (Figure 3b), which shows the worst reproducibility comparing with other peaks. It was reported that there is a transformation from P2 phase to O2 phase starting at ~4.2 V since O2-type stacking faults were introduced into the P2 structure.[39] The transformation is obviously partly reversible and may cause severe structural distortion, which may cause great capacity fade. If the low cut-off voltage was set to 1.5 V, according to the reported studies and the obvious oxidation/reduction peaks appearing below 2.0 V (Figure 3b), it can be concluded that $Mn^{4+}$ was activated and reduced to $Mn^{3+}$ after the initial $Na^+$ ions insertion. $Mn^{4+}/Mn^{3+}$ redox pair is responsible for the redox peaks below 2.0 V. The formation of Jahn-Teller active $Mn^{3+}$ results in large structural distortions of $MnO_6$ octahedra which can induce constraints and defects in the active material, leading to increased capacity fading.[26] $Mn^{3+}$ undergoes the disproportion reaction forming $Mn^{4+}$ and $Mn^{2+}$ ($2Mn^{3+}_{solid}$ $Mn^{4+}_{solid}$ + $Mn^{2+}_{electrolyte}$) and continuous decomposition of the electrolyte at high voltages. Furthermore, the $Mn^{2+}$ is easily dissolved in the electrolyte which would cause a constant degradation of the active material.[42] More obvious peaks at around 2.0 V than that in Figure 3a suggests a possibility of occurrence of new phase transformation. It can be expected that the electrodes may experience big capacity fade if continually cycled to 4.5 V or 1.5 V.

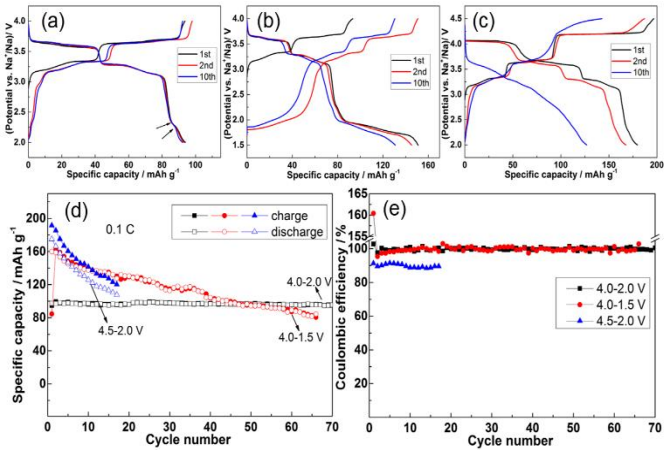


**Figure 4.** (a-c) Charge-discharge profiles, (d) cycling performance and (e) corresponding coulombic efficiency of Na/NNMO cell at different cut-off voltages at 0.1 C.

**Figure 4** shows the charge-discharge profiles and electrochemical performance of NNMO cycling at 0.1 C. The charge-discharge cut-off voltages are set to 4.0/2.0, 4.0/1.5 and 4.5/2.0 V to study the effect of high or low voltage on the electrochemical performance of Na/NNMO cell. It can be seen that the charge-discharge cut-off voltage is crucial for the capacity retention and coulombic efficiency of the electrodes. The plateau in the charge-discharge profiles are consistent with the characteristic peaks in the CV curves, and show different degrees of reproducibility during cycling processes under different cut-off voltage ranges.

When performing between 4.0 and 2.0 V (Figure 4a and d), several voltage plateaus corresponding to the CV peaks are observed, caused by the different staging of the sodium layers.[43] The initial charge and discharge capacity were 93.3 and 93.0 mAh $g^{-1}$, corresponding to the extraction of 0.360 mol and the insertion of 0.358 mol of $Na^+$ ions per formula unit, respectively. Thus, the x value in $Na_xNi_{1/3}Mn_{2/3}O_2$ was maintained at approximately 0.67, and $Na^+$ could be extracted and inserted reversibly after several charge-discharge cycles, which well explains the excellent cyclability of Na/NNMO cell in Figure 4d. The Coulombic efficiency (CE) in the first and following cycles almost equal to 100% during the whole cycling process. There is no visible decay and the capacity retention is 95.7% after 100 cycles.

In the voltage range of 4.0 and 1.5 V (Figure 4b and d), the electrode cycled reversibly with slight capacity decay, but the voltage steps were still reproducible throughout the whole test. Comparing with cells cycling between 4.0 and 2.0 V, another long flat voltage slope at ~1.75 V which associated with the redox reaction of the $Mn^{4+}/Mn^{3+}$ pairs, was observed. The initial discharge capacity was increased to 151.0 mAh $g^{-1}$, of which ~38.4% (58 mAh $g^{-1}$) was contributed by the insertion of $Na^+$ below 2 V. The x value in $Na_xNi_{1/3}Mn_{2/3}O_2$ cycling in the range of 4.0-1.5 V was increased to 0.95 at the end of discharge process after 0.58 mol of Na ions extracted during the charge process per formula unit. This over-insertion of $Na^+$ ions reaches the theoretical $Na^+$ intercalation limit where the oxidation state of Mn is totally $Mn^{3+}$.[37, 44] The CE was 160% in the first cycle and kept stable at ~99% from the second cycle. Faster capacity fading was observed than that between 4.0-2.0 V due to the increasing distortion of $MnO_6$ octahedra caused by increasing number of $Mn^{3+}$ ions, which can induce constraints, defects and thus structural deterioration of the material.[26]

In Figure 4c and d, the initial charge capacity of NNMO was increased to 191.5 mAh $g^{-1}$ when cell was charged to 4.5 V, 18.5 mAh $g^{-1}$ higher than the theoretical capacity due to possible electrolyte decomposition above 4.4 V. A long plateau at 4.18 V indicated the occurrence of a two-phase reaction, corresponding to the P2-O2 phase transformation. There was a strong capacity fade during cycling. While 0.70 $Na^+$ ions per formula unit were reintercalated in the first discharge process, only 0.52 $Na^+$ ions were reversibly cycled in the $10^{th}$ cycle. After 10 cycles, the long plateau at ~3.7 V almost disappeared and the capacity retention was only 71.8%. Furthermore, the CE during the whole cycling was much lower and only reached ~90%. The severe capacity fade and

low CE could originate from the increasing catalytic decomposition of the electrolyte with increased charging voltage and the increasing irreversibility of the electrode material associated to structural changes.[45]. The P2-O2 phase transition induces large volume shrinkage ( ~23%) caused by an oxygen framework shift, which would cause fast capacity decay during the cycles in $Na_xNi_{1/3}Mn_{2/3}O_2$.[27]

It was found that a low 1.5 V or high 4.5 V cut-off voltage does not lead to capacity improvement for long-term cycling, since after about 10 or 60 cycles the capacity value of the cell with $E_{cut\text{-}off}$ = 4.0/2.0 V is reached due to the redox reaction of the $Mn^{4+}/Mn^{3+}$ ionic pair below 2 V or P2-O2 transformation and electrolyte decomposition above 4.2 V. Meanwhile, the cycling performance of NNMO at 1 C was also characterized at different cut-off voltages and is shown in Figure S4. Similar capacity changing trends were found. Interestingly, the CE in the voltage of 4.5-2.0 V was higher than that at 0.1 C. The lower CE at 0.1 C is probably due to the continuous formation of SEI layer for longer time and slower sodium ions diffusion at lower current rate. High current density, to some extent, inhibits the occurrence of side reaction due to the fast sodium ion de-insertion/insertion processes.

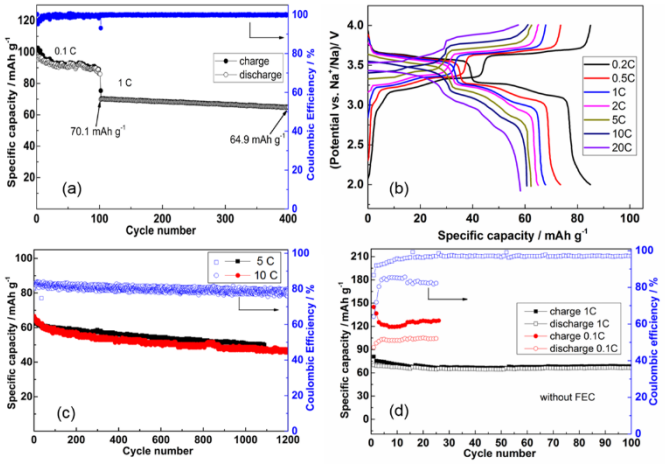


**Figure 5**. Electrochemical properties of Na/NNMO cell between 4.0 and 2.0 V: (a) cycling performance and corresponding coulombic efficiency at 0.1 C and 1 C, (b) rate capacity, (c) cycling performance and corresponding coulombic efficiency at 5 C and 10 C and (d) cycling performance and corresponding coulombic efficiency using electrolyte without FEC additive.

We then focus on the electrochemical properties of NNMO at 4.0/2.0 V, during which there is no phase transformation from P2 to O2 or formation of $Mn^{3+}$, and the electrode exhibits excellent cycling stability and high coulombic efficiency. **Figure 5**a shows the cycling performance of NNMO at 0.1 C and 1 C. After 100 cycles, the discharge capacity retains 89.0 mAh $g^{-1}$ at 0.1 C, corresponding to a capacity retention of 95.7% of the first cycle. Moreover, the capacity retention at 1 C after 300 cycles can reach 92.6%. Again, the CE at both current densities are stable and remain almost 100%. The increasing current densities will not deteriorate the CE of NNMO. This phenomenon indicates high current density can only cause polarization but will not intensify the side reactions.[46] In the rate capacity shown in Figure 5b, the specific capacity reduced gradually with increasing rate, which could be ascribed to an increase in overpotential resulting from less reaction time for the free cation intercalation into the crystal lattice. In details, the discharge capacities are 84.9, 73.5, 67.8, 65.1 62.2, 60.7, and 58.2 mAh $g^{-1}$ at 0.2, 0.5, 1, 2, 5, 10, and 20 C respectively. The voltage plateaus could be clearly seen at high current densities. Meanwhile, the NNMO electrodes exhibit excellent cycling stability at high current densities of 5 and 10 C, as shown in the Figure 5c. The capacity retention is 71.2% even after 1200 cycles at 10 C.

We also study the effect of FEC additive in the electrolyte on the electrochemical performance of NNMO electrode. As shown in Figure 5d, without the addition of FEC, the reversible discharge capacity did not change much comparing with that with FEC additive. The charge capacity, however, are 110 and 79 mA $g^{-1}$ at 0.1 C and 1 C respectively, which are higher than those using FEC additive, resulting in lower coulombic efficiencies. It was reported that FEC additive can suppress the electrolyte decomposition, enhance the reversibility of Na and improve the SEI passivation capability,[47,48] thus decreasing the occurrence of irreversible capacity. Again, the CE at 1 C is higher than that at 0.1 C due to the faster sodium ions diffusion. Comparison of electrochemical performances among reported P2-type $Na_{2/3}Ni_{1/3}Mn_{2/3}O_2$ materials are made and shown in Table S2.

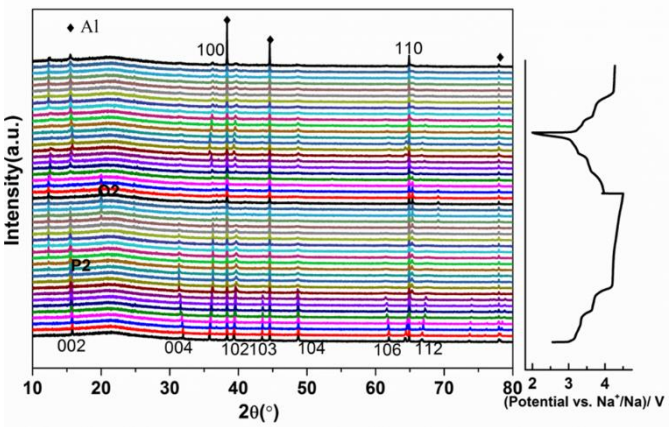


**Figure 6.** *In-suit* synchrotron XRD patterns of NNMO cycling between 4.5 and 2.0 V at 0.5 C, the 2θ has been converted based on the Cu wavelength for convenience.

*In-suit* synchrotron XRD was performed to study the evolution of NNMO during cycling between 4.5-2.0 V and is shown in **Figure 6**. The pristine $Na_{2/3}Ni_{1/3}Mn_{2/3}O_2$ has an ordered hexagonal structure. During the charging process, the (00*l*) peaks shift to a lower angle with decreasing intensity, indicating the expansion of sodium content sensitive *c* parameter and thus the interplanar distance. The decrease of *a* parameter is indicated by the shift of the (100) peak to higher angles. The successive extraction of $Na^+$, which is located between the transition metal layers, leads to a large repulsion of the oxygen anions and, therefore, results in the increase of the *c*-axis parameter as well as the decrease of *a* parameter,[43] in agreement with the investigation by Lu *et al*.[23] While the (100), (102), (103), (110) and (112) peaks moved to higher angles, the (104) and (106) peaks in our study moved to lower angles. This evolution is different with the former report,[23] in which all (10*l*) peaks shift to a lower angle, indicating the different evolution degrees of lattice parameters. All the peaks became broader with decreasing intensity along with the extraction of sodium ions. There is no new phase formed and only solid-solution behaviour occurs below 3.8 V. Multiple new Bragg peaks observed at 21 and 70˚ were formed above 4.2 V, indicating the formation of O2 phase, which is in agreement with the previous report.[23] It was reported that the transition metal oxide ($TMO_2$) slabs would glide to form octahedral sites after extraction of the $Na^+$ ions, leading to the formation of a new O2-type phase with stacking faults and a unique oxygen packing.[41] The (100) split and (10*l*) peaks become broader as more O2 stacking faults are introduced in the slabs.[49] But another phase appearing at 4.0 V indicated by the peaks at ~12 and 25˚ might be attributed to the intercalation of water, solvent molecules and/or salt ions in the interstitial space between the $TMO_2$ slabs.[50-51] And the intercalation is reversible in the 2nd cycle. It was reported that there was Z phase formed during the charge to 4.3 V of $Na_{2/3}Ni_{1/3}Mn_{2/3}O_2$.[35] However, there is no Z phase observed in our study. The progressive disappearance of the high-voltage plateau above 4.25 V upon cycling (Figure 4c) suggests that the transition to O2 phase might be responsible for the capacity fading. Similar phenomena were also observed in some other P2 type cathode materials and O3 type layered compounds.[13, 15, 23, 49, 52-54]

Upon discharging, the O2 phase gradually disappeared and a reversible evolution took place. The Bragg diffraction peaks shifted to the opposite direction to that of the charge process, indicating a reversible structural evolution during the charge/discharge process. However, the intensity of peaks decreased and could not return to its primary phase, indicating big irreversibility which would result in great capacity fading during the de-insertion/insertion of $Na^+$ ions. As $Na^+$ inserts between the $MnO_6$ layers, the negative charges of the oxygen between different layers are screened, which moves the layers closer together, leading to the decrease of *c* parameter. The (100) shift to lower angle reflects the expansion of *a* and *b* parameters, resulting from a decrease of the oxidation state of manganese and thus an expansion of the $MnO_6$-octahedra during discharge.[17]

*In-suit* synchrotron XRD of NNMO cycling between 4.0-1.5 V was also characterized to study the evolution in low voltage area (Figure S5). In the initial charge to 4.0 V, the evolution is the same with Figure 6. Only solid solution mechanism occurred during this voltage range. Limit the voltage to 4.0 V excludes the formation of O2 phase and electrolyte decomposition, resulting in slower capacity fading compared with that of being charged to 4.5 V. During the following discharge process, a solid solution mechanism was observed at the beginning. However, when discharged to or below 2.0 V, the (002), (100), (102) and (112) peaks split into two peaks along with the decrease of peak intensities, which is indicative of a biphasic mechanism. The appearance of two diffraction peaks at about 15.9 and 32.0˚ correspond to the $(002)_{P2}$ and $(004)_{P2}$ reflections in the hexagonal pattern.[52] The appearance of a small new phase (orthorhombic P2' phase) below 2.0 V is attributed to increasing distortion caused by the increasing concentration of $Mn^{3+}$ formed from reduction of $Mn^{4+}$. The biphasic domain between the P2 and P2' phase is observed for a Na content of $0.85< x<0.95$ in $Na_xNi_{1/3}Mn_{2/3}O_2$.[52, 55] The bi-phasic mechanism here is reversible and the phase return to its initial situation during the discharge process.

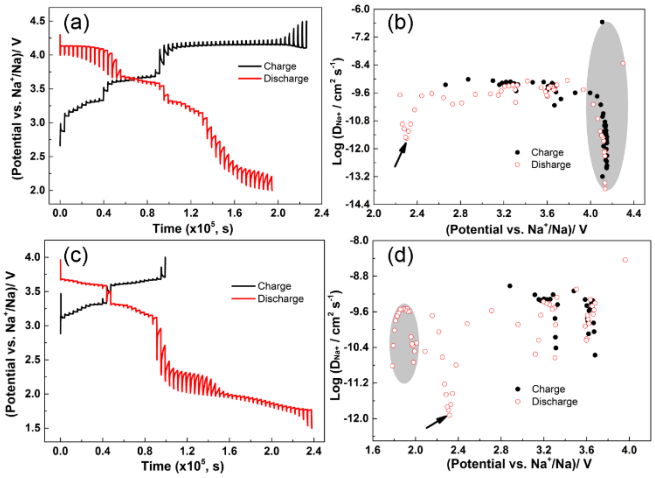


**Figure 7**. (a) GITT curves for the charge and discharge states of the first cycle and (b) corresponding sodium-ion diffusion coefficient ($D_{Na+}$) of Na/NNMO cell cycling between 4.5 and 2.0 V; (c) GITT curves for the charge and discharge states of the first cycle and (d) corresponding $D_{Na+}$ of Na/NNMO cell cycling between 2.0 and 1.5 V.

**Figure 7** shows the GITT curves for the first cycle at 0.1 C of Na/NNMO cell and the corresponding sodium-ion diffusion coefficient ($D_{Na+}$) with different cut-off voltages. It is found that the $D_{Na+}$ values are highly related to the phase transformation and structural evolution during the charge-discharge process. The $D_{Na+}$ were stable with a high value of ~$10^{-10}$ $cm^2$ $s^{-1}$ at the beginning of Na extraction during charge process (Figure 7b and d) and began to drop obviously at the phase transformation area (P2-O2, grey area). The value was only $6.39 \times 10^{-14}$ $cm^2$ $s^{-1}$ when charged to 4.5 V. Upon discharging, both $D_{Na+}$ show a minimum (~$10^{-12}$ $cm^2$ $s^{-1}$) as the arrows indicate due to the $Na^+$/vacancy ordering at around 2.3 V, corresponding to the CV peaks and voltage plateaus between 3.0-2.0 V. Similarly, $D_{Na+}$ began to drop when the P2-P2' transformation happened below 2.0 V (grey area) in Figure 7d.

Meanwhile, the $D_{Na+}$ of NNMO was also investigated by electrochemical impedance spectroscopy for electrodes before and after 700 cycles at 1 C between 4.0-2.0 V. The Nyquist curves and the corresponding $Z_{re}$ vs $\omega^{-1/2}$ plots in the low-frequency region are shown in Figure S6. Values of fitted parameters are shown in Table S3. The $D_{Na+}$ calculated for electrodes are $9.02\times10^{-12}$ and $7.15\times10^{-12}$ $cm^2$ $s^{-1}$, respectively. The high $D_{Na+}$ values well explain the excellent cycling performance of the prepared NNMO. Even after cycling for 1000 cycles at 1 C, the layered structure of NNMO can still be observed in the electrode (Figure S7), indicating its superior structure stability.

## Conclusion

In summary, layered P2-type $Na_{2/3}Ni_{1/3}Mn_{2/3}O_2$ was successfully synthesized through a facile sol-gel method and subsequent heat treatment. Resulting from different phase transformation and sodium ion diffusion rate, the electrochemical performance is highly related to the cut-off voltage and the electrolyte used. When the cut-off voltage is set up to 4.5 V or lowered to 1.5 V, capacity fade happens due to the occurrence of P2-O2 transformation and electrolyte decomposition or the redox reaction of the $Mn^{4+}/Mn^{3+}$ ionic pair and P2-P2' transformation. The electrode maintained 89.0 mAh $g^{-1}$ with good cycling stability and excellent structural preservation between 4.0-2.0 V. The capacity retention is 71.2% even after 1200 cycles at 10 C. It can be expected that P2-type $Na_{2/3}Ni_{1/3}Mn_{2/3}O_2$ is very promising as a cathode material for sodium ion battery.

## Conflicts of interest

There are no conflicts to declare.

## Acknowledgements

This work is financially supported by the Australian Renewable Energy Agency (ARENA) Project grant and and the funds from the National Natural Science Foundation of China (51572199 and 51772218). The authors are grateful to Dr. Tania Silver for her critical revision of the manuscript. The authors also acknowledge the use of the facilities in the UOW Electron Microscopy Centre.

## References

1. Z. Yang, J. Zhang, M. C. Kintner-Meyer, X. Lu, D. Choi, J. P. Lemmon, J. Liu, *Chem. Rev.,* 2011, **111**, 3577-3613.
2. B. Dunn, H. Kamath, J.-M. Tarascon, *Science,* 2011, **334**, 928-935.
3. J. Deng, W.-B. Luo, S.-L. Chou, H.-K. Liu, S.-X. Dou, *Adv. Energy Mater.*, 2018, **8**, 1701428.
4. X. Xiang, K. Zhang, J. Chen, *Adv. Mater.,* 2015, **27**, 5343-5364.
5. H. Hou, C. E. Banks, M. Jing, Y. Zhang, and X. Ji, *Adv. Mater.* 2015, **27**, 7861-7866.
6. H. Hou, L. Shao, Y. Zhang, G. Zou, J. Chen, and X. Ji, *Adv. Sci.* 2017, **4**, 1600243.
7. N. Yabuuchi, K. Kubota, M. Dahbi, S. Komaba, *Chem. Rev.,* 2014, **114**, 11636-11682.
8. Q. Liu, Z. Hu, M. Chen, Q. Gu, Y. Dou, Z. Sun, S.-L. Chou, S. X. Dou, *ACS Appl. Mater. Interfaces,* 2017, **9**, 3644-3652.
9. Z. Gong, Y. Yang, *Energy Environ. Sci.,* 2011, **4**, 3223-3242.
10. J. Xu, F. Lin, M. M. Doeff, W. Tong, *J. Mater. Chem. A*, 2017, **5**, 874-901.
11. Y. Fang, X.-Y. Yu, X. W. Lou, *Angew. Chem. Int. Ed.* 2017, **56**, 5801-5805.
12. S. P. Ong, V. L. Chevrier, G. Hautier, A. Jain, C. Moore, S. Kim, X. Ma, G. Ceder, *Energy Environ. Sci.,* 2011, **4**, 3680-3688.
13. E. Talaie, V. Duffort, H. L. Smith, B. Fultz, L. F. Nazar, *Energy Environ. Sci.,* 2015, **8**, 2512-2523.
14. C. Delmas, C. Fouassier, P. Hagenmuller, *Phys. B + C,* 1980, **99**, 81-85.
15. N. Yabuuchi, M. Kajiyama, J. Iwatate, H. Nishikawa, S. Hitomi, R. Okuyama, R. Usui, Y. Yamada, S. Komaba, *Nat. Mater.,* 2012, **11**, 512-517.
16. J. Hwang, S. Myung, Y. Sun, *Chem. Soc. Rev.,* 2017, **46**, 3529-3614.
17. N. Bucher, S. Hartung, J. B. Franklin, A. M. Wise, L. Y. Lim, H.-Y. Chen, J. N. Weker, M. F. Toney, M. Srinivasan, *Chem. Mater.,* 2016, **28**, 2041-2051.
18. N. Yabuuchi, R. Hara, M. Kajiyama, K. Kubota, T. Ishigaki, A. Hoshikawa, S. Komaba, *Adv. Energy Mater.,* 2014, **4**, 1301453.
19. J. Paulsen, J. Dahn, *Solid State Ionics,* 1999, **126**, 3-24.
20. S. Y. Lee, J. H. Kim, Y. C. Kang, *Electrochim. Acta,* 2017, **225**, 86-92.
21. T. Risthaus, D. Zhou, X. Gao, X. He, B. Qiu, J. Wang, L. Zhang, Z. Liu, E. Paillard, G. Schumacher, M. Winter, J. Li, *J. Power Sources,* 2018, **395**, 16-24.
22. H. V. Ramasamy, K. Kaliyappan, R. Thangavel, V. Aravindan, K. Kang, D. U. Kim, Y. Park, X. Sun, Y.-S. Lee, *J. Mater. Chem. A*, 2017, **5**, 8408-8415.
23. Z. Lu, J. Dahn, *J. Electrochem. Soc.,* 2001, **148**, A1225-A1229.
24. H. Wang, M. Gu, J. Jiang, C. Lai, X. Ai, *J. Power Sources,* 2016, **327**, 653-657.
25. P. Manikandan, D. Ramasubramonian, M. Shaijumon, *Electrochim. Acta,* 2016, **206**, 199-206.
26. J. Yoshida, E. Guerin, M. Arnault, C. Constantin, B. M. de Boisse, D. Carlier, M. Guignard, C. Delmas, *J. Electrochem. Soc.,* 2014, **161**, A1987-A1991.
27. L. Wang, Y.-G. Sun, L.-L. Hu, J.-Y. Piao, J. Guo, A. Manthiram, J. Ma, A.-M. Cao, *J. Mater. Chem. A*, 2017, **5**, 8752-8761.
28. H. Hou, B. Gan, Y. Gong, N. Chen, C. Sun, *Inorg. Chem.,* 2016, **55**, 9033-9037.
29. Z. Lu, J. Dahn, *J. Electrochem. Soc.,* 2001, **148**, A710-A715.
30. Z. Lu, J. Dahn, *Chem. Mater.,* 2001, **13**, 1252-1257.
31. L. Liu, X. Qi, Q. Ma, X. Rong, Y. Hu, Z.-B. Zhou, H. Li, X. Huang, L. Chen, *ACS Appl. Mater. Interfaces,* 2016, **8**, 32631-32636.
32. J. Paulsen, R. Donaberger, J. Dahn, *Chem. Mater.,* 2000, **12**, 2257-2267.
33. J. Billaud, G. Singh, A. R. Armstrong, E. Gonzalo, V. Roddatis, M. Armand, T. Rojo, P. G. Bruce, *Energy Environ. Sci.,* 2014, **7**, 1387-1391.
34. X. Wang, M. Tamaru, M. Okubo, A. Yamada, *J. Phys. Chem. C,* 2013, **117**, 15545-15551.
35. X. Wu, G.-L. Xu, G. Zhong, Z. Gong, M. J. McDonald, S. Zheng, R. Fu, Z. Chen, K. Amine, Y. Yang, *ACS Appl. Mater. Interfaces,* 2016, **8**, 22227-22237.
36. X. Wu, J. Guo, D. Wang, G. Zhong, M. J. McDonald, Y. Yang, *J. Power Sources,* 2015, **281**, 18-26.
37. Y. Wen, B. Wang, G. Zeng, K. Nogita, D. Ye, L. Wang, *Chem. Asian J.,* 2015, **10**, 661-666.
38. K. Kang, Y. S. Meng, J. Bréger, C. P. Grey, G. Ceder, *Science,* 2006, **311**, 977-980.
39. D. H. Lee, J. Xu, Y. S. Meng, *Phys. Chem. Chem. Phys.,* 2013, **15**, 3304-3312.
40. X. Ma, H. Chen, G. Ceder, *J. Electrochem. Soc.,* 2011, **158**, A1307-A1312.
41. P. F. Wang, Y. You, Y. X. Yin, Y. S. Wang, L. J. Wan, L. Gu, Y. G. Guo, *Angew. Chem. Int. Ed.,* 2016, **55**, 7445-7449.
42. C. Luo, A. Langrock, X. Fan, Y. Liang, C. Wang, *J. Mater. Chem. A*, 2017, **5**, 18214-18220.
43. D. Buchholz, A. Moretti, R. Kloepsch, S. Nowak, V. Siozios, M. Winter, S. Passerini, *Chem. Mater.,* 2013, **25**, 142-148.
44. M. H. Han, E. Gonzalo, N. Sharma, J. M. López del Amo, M. Armand, M. Avdeev, J. J. Saiz Garitaonandia, T. Rojo, *Chem. Mater.,* 2015, **28**, 106-116.
45. M. Sathiya, K. Hemalatha, K. Ramesha, J.-M. Tarascon, A. Prakash, *Chem. Mater.,* 2012, **24**, 1846-1853.
46. Y. Bai, L. Zhao, C. Wu, H. Li, Y. Li, F. Wu, *ACS Appl. Mater. Interfaces,* 2016, **8**, 2857-2865.
47. S. Komaba, T. Ishikawa, N. Yabuuchi, W. Murata, A. Ito, Y. Ohsawa, *ACS Appl. Mater. Interfaces,* 2011, **3**, 4165-4168.
48. M. Dahbi, T. Nakano, N. Yabuuchi, S. Fujimura, K. Chihara, K. Kubota, J. Y. Son, Y. T. Cui, H. Oji, S. Komaba, *ChemElectroChem,* 2016, **3**, 1856-1867.
49. X. Li, D. Wu, Y.-N. Zhou, L. Liu, X.-Q. Yang, G. Ceder, *Electrochem. Commun.,* 2014, **49**, 51-54.
50. D. Buchholz, L. G. Chagas, C. Vaalma, L. Wu, S. Passerini, *J. Mater. Chem. A,* 2014, **2**, 13415-13421.
51. P.-F. Wang, Y. You, Y.-X. Yin, Y.-G. Guo, *J. Mater. Chem. A,* 2016, **4**, 17660-17664.
52. B. Mortemard de Boisse, D. Carlier, M. Guignard, L. Bourgeois, C. Delmas, *Inorg. Chem.,* 2014, **53**, 11197-11205.
53. D. Yang, X.-Z. Liao, J. Shen, Y.-S. He, Z.-F. Ma, *J. Mater. Chem. A*, 2014, **2**, 6723-6726.
54. Y. Xie, H. Wang, G. Xu, J. Wang, H. Sheng, Z. Chen, Y. Ren, C. J. Sun, J. Wen, J. Wang, *Adv. Energy Mater.,* 2016, **6**, 1601306.
55. J.-P. Parant, R. Olazcuaga, M. Devalette, C. Fouassier, P. Hagenmuller, *J. Solid State Chem.,* 1971, **3**, 1-11.